A Seismogeodetic Amphibious Network in the Guerrero Seismic Gap, Mexico

by Víctor M. Cruz-Atienza, Yoshihiro Ito, Vladimir Kostoglodov, Vala Hjörleifsdóttir, Arturo Iglesias, Josué Tago, Marco Calò, Jorge Real, Allen Husker, Satoshi Ide, Takuya Nishimura, Masanao Shinohara, Carlos Mortera-Gutierrez, Soliman García, and Motoyuki Kido

ABSTRACT

The historical record of large subduction earthquakes in Guerrero, Mexico, reveals the existence of an ~230–km length segment below the coast where no major rupture has occurred in the past 60 years. Reliable quantification of the hazard associated with such a seismic gap is urgently needed for risk mitigation purposes by means of state-of-the-art observations and modeling. In this article, we introduce and quantitatively assess the first seismogeodetic amphibious network deployed in Mexican and Central American soils that will provide the opportunity to achieve this goal in the near future. Deployed in 2017, the network is the result of a collaborative effort between Mexican and Japanese scientists. It consists of 15 onshore broadband and 7 ocean-bottom seismometers, 33 Global Positioning System (GPS) stations, 7 ocean-bottom pressure gauges, and 2 GPS-acoustic sites, most of them installed within the Guerrero seismic gap. Initial data from the network revealed the occurrence of a 6-month-long slow-slip event in Guerrero, starting in May and ending in October 2017. To illustrate the performance of the various instruments, we also present the first ocean-bottom pressure and GPS-acoustic measurements in Mexico; the latter was obtained by means of an autonomous Wave Glider vehicle. The ground motion of the devastating 19 September 2017 M_w 7.1 earthquake in central Mexico is presented as well. Nominal resolution of the seismogeodetic network is estimated through different synthetic inversion tests for tomographic imaging and the seismic coupling (or slow-slip) determination on the plate interface. The tests show that combined onshore and offshore instruments should lead to unprecedented results regarding the seismic potential (i.e., interface coupling) of the seismic gap and the Earth structure from the Middle America trench up to 70-km depth across the Guerrero state.

INTRODUCTION

Three major subduction thrust earthquakes since 2004 with $M_w \geq 8.8$ (Lay *et al.*, 2012) and the associated humanitarian tragedies around the world have raised fundamental questions in the communities devoted to understanding hazard assessment and the physics of earthquakes. Among the lessons learned from these events include accepting the possibility of future ruptures much larger than those documented in the historical records of any subduction zone. Disaster risk assessment and prevention from these kinds of scenarios require new and more sophisticated observational facilities aiming to monitor any tectonic manifestation related to the seismic cycle. Data recorded in the vicinity of the seismogenic faults may lead to unprecedented quantification of the earthquake potential and constraints for physics-based models (i.e., models integrating constitutive laws for the fault friction, the fluids thermal pressurization, and the rocks rheology), leading to more reliable hazard assessments.

As revealed by past events (Fig. 1), seismicity along the Pacific coast of Mexico produced by the interaction of the subducting Cocos plate and the overriding North American plate represents a high risk of disaster related to megathrust earthquakes and tsunamis (e.g., 1985 M_w 8.0: Anderson *et al.*, 1986; and 1787 $M_w \sim 8.6$: Suárez and Albini, 2009). In particular, an ~230–km–long segment of the Mexican subduction zone offshore and below the coast of the state of Guerrero has not broken in a significant rupture ($M_w \geq 7.2$) in at least 60 years. Recent earthquakes that occurred in April (Papanoa, M_w 7.3) and May (M_w 6.5 and 6.1) 2014 on the Costa Grande of the state (west from Acapulco, Figs. 1 and 2) are a reminder of what has been preparing for more than 106 years in that 130-km-long segment of the seismic gap between Acapulco and Papanoa (Fig. 2). Whereas the main event initiated outside the gap and halted right in its western edge, the May events broke within the gap (National Autonomous University of Mexico [UNAM] Seismology Group, 2015). East of Acapulco, below (and offshore) the Costa Chica of the state (Fig. 2), another ~100–km–long segment extends where the last major earthquake occurred in 1957 (Duke and Leeds, 1959; Singh *et al.*, 1982). Considering that (1) the return period by segment for major ($M_w \geq 7.2$) subduction earthquakes in Mexico ranges between 30 and 60 years (Singh *et al.*, 1981) and that (2) only between 1899 and 1911, a sequence of seven large and very large earthquakes occurred in the Costa Grande region (all of them with a magnitude larger than or equal to 7 and a maximum

doi: 10.1785/0220170173

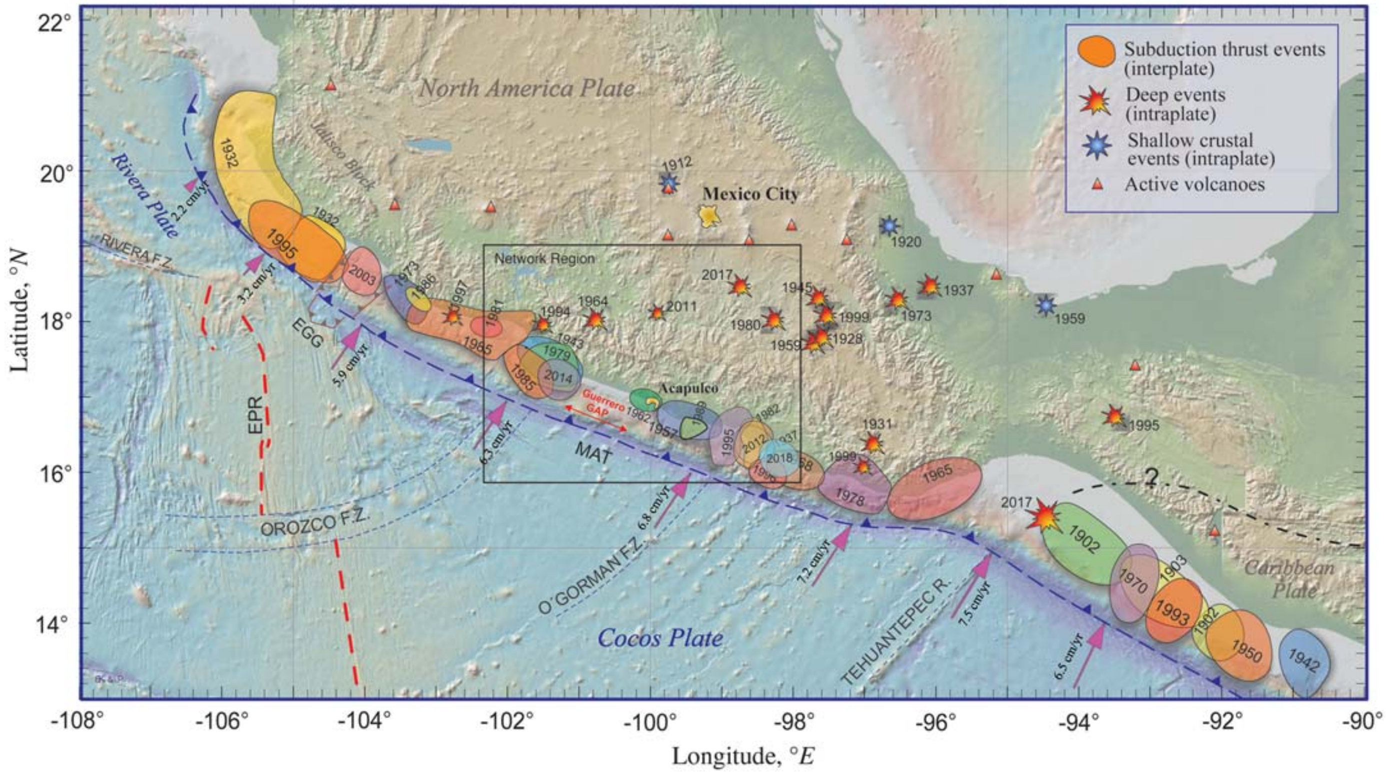

▲ **Figure 1.** Map showing the tectonic setting of central Mexico and the main rupture areas and epicenters of large earthquakes since 1900 (modified from Kostoglodov and Pacheco, 1999).

magnitude of 7.9) (UNAM Seismology Group, 2015), the specialists believe that an $M_w \approx 8.2$ earthquake with an ~230–km–long rupture in the extended Guerrero seismic gap (GGap) (Fig. 2) is a severe but plausible scenario for the near future. Such a rupture could produce pseudospectral velocities for periods around 3 s in Mexico City two to three times larger than those experienced during the devastating 1985 M_w 8.0 Michoacán earthquake (Kanamori *et al.*, 1993), which killed ~10,000 people in the capital where more than 22 million people live today.

Detailed investigations of the three worldwide megathrust earthquakes referred to earlier have revealed that most of the seismic moment in all cases was released in the offshore part of the plate interface, close to the trench where seismic coupling is supposed to be relatively low, raising fundamental questions about the nature of the rupture process in subduction zones (see Lay *et al.*, 2012, and references therein). We know little about the plate-interface processes taking place between the Middle American trench and the coast of Mexico, where the expected large rupture in Guerrero may produce a disastrous tsunami similar to the one in 1787 along the coast of Oaxaca caused by an $M_w \sim 8.6$ event (Núñez-Cornú *et al.*, 2008; Suárez and Albini, 2009), as revealed by paleoseismological data suggesting that large tsunamis could have happen in the late Holocene along the coasts there (Ramirez-Herrera *et al.*, 2007). In Japan and Chile, for example, offshore slow-slip transients have occurred prior to major events (Kato *et al.*, 2012; Ito *et al.*, 2013; Ruiz *et al.*, 2014). The same could happen with the occurrence of tectonic tremor and very low-frequency earthquakes (Ito *et al.*, 2015; Yamashita *et al.*, 2015). Thus, slow earthquakes seem to significantly affect the strain accumulation in the seismogenic zone. In the state of Guerrero, long-term slow-slip events (SSEs) occur approximately every 3.5 years (Cotte *et al.*, 2009) and represent the largest documented aseismic events in the world, with equivalent moment magnitudes up to 7.6 (Kostoglodov *et al.*, 2003). Estimates of the seismic coupling in the plate interface suggest that the long-term strain-rate accumulation in the Costa Grande segment of the GGap is 75% lower than in the adjacent regions (e.g., the Costa Chica; Radiguet *et al.*, 2012). Remarkably, the stress perturbation induced by these transients could also lead to the rupture of dynamically mature asperities, as suggested during the April 2014 M_w 7.3 Papanoa earthquake (Radiguet *et al.*, 2016), for which the rupture began during the development of an SSE in the region (UNAM Seismology Group, 2015). Tectonic tremor, low-frequency, and very low-frequency earthquakes have also been observed in Guerrero close to the plate interface at 40- to 45-km depth during the occurrence of SSEs (Payero *et al.*, 2008; Kostoglodov *et al.*, 2010; Husker *et al.*, 2012; Frank *et al.*, 2014; Cruz-Atienza *et al.*, 2015; Maury *et al.*, 2016; V. M. Cruz-Atienza *et al.*, unpublished manuscript, 2018, see Data and Resources), suggesting that such phenomena are causally related (Villafuerte and Cruz-Atienza, 2017) as postulated for other subduction zones (e.g., Hirose and Obara, 2010; Bartlow *et al.*, 2011).

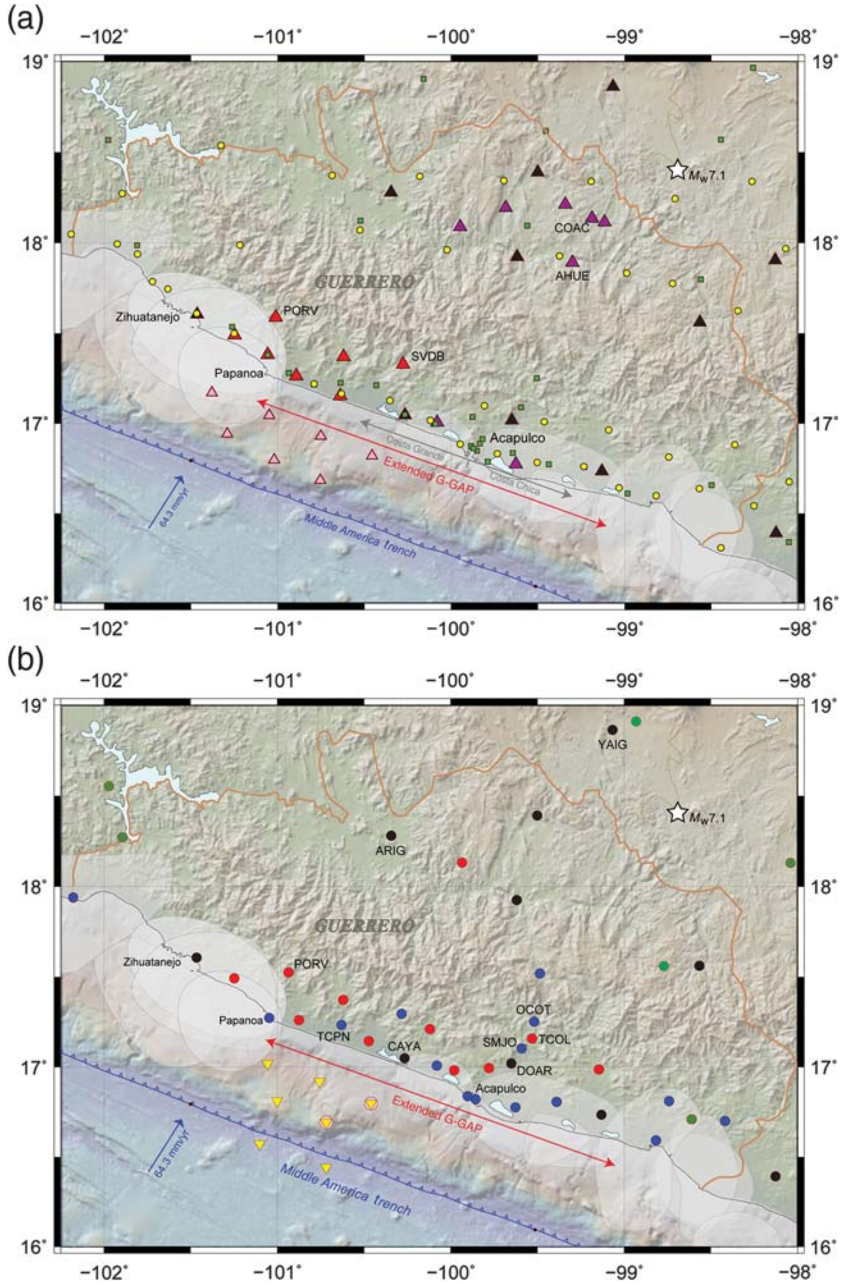

▲ **Figure 2.** (a) Seismological and (b) geodetic amphibious network in the Guerrero seismic gap (GGap) and nearby regions. Broadband seismic stations provided by Japan (red triangles), broadband seismic stations from Mexico-National Autonomous University of Mexico (UNAM) (purple triangles), broadband and strong motion from the Servicio Sismológico Nacional (SSN)-UNAM (black triangles), ocean-bottom seismometers (OBSs) from Japan (pink triangles), strong-motion stations from the Institute of Engineering-UNAM (green squares), and strong-motion stations from Centro de Instrumentación y Registro Sísmico (CIRES)-SASMEX (yellow circles). Global Positioning System (GPS) stations from Japan (red circles), GPS stations from Mexico-UNAM (blue circles), GPS stations from the SSN-UNAM (black circles), GPS stations from TLALOCNet Mexico-UNAM (green circles), ocean-bottom pressure gauges (OBPs) stations from Japan–Mexico (yellow triangles), and GPS-acoustic (GPS-A) arrays from Japan–Mexico (pink circles). Shaded areas represent the approximate rupture areas from large earthquakes since 1911 (modified from Kostoglodov and Pacheco, 1999), and the white star indicates the epicenter of the 19 September 2017 M_w 7.1 intermediate-depth earthquake.

Understanding this phenomenology, which is present in different subduction zones around the globe, results in the critical importance to produce reliable hazard assessments for future earthquakes and tsunamis and thus to mitigate the associated risk. Achieving this goal in Guerrero requires addressing fundamental questions such as, how does the long-term seismic coupling evolve with time from the trench up to 40-km depth? Do SSEs, tectonic tremor, and small (e.g., repeating) earthquakes occur near the trench? How do they behave? How far do the long-term SSEs penetrate into the seismogenic zone of the GGap? What are the mechanical properties of the plate interface in the shallow transition zone? Are there pressurized fluids in it? What are the elastic properties and geometry of the subducting Cocos plate? What is the probability of a next megathrust event in the GGap? What could be its maximum slip near the trench, and how large would be the associated ground motion and tsunami? Robust answers to these questions are only possible using data from a seismogeodetic network overlying the plate interface from the trench (offshore) to inland regions far enough from the coast. This is by means of seismic and geodetic stations encompassing the seismogenic zone and both the up-dip and down-dip transition zones of the plate interface.

Physics-based earthquake and tsunami scenarios in the GGap constrained by state-of-the-art observations, both onshore and offshore, are thus urgently needed for disasters mitigation caused by future megathrust earthquakes in the Pacific coast of Mexico. To achieve this goal, we installed in 2017 a seismogeodetic amphibious network in the region. The network is composed of seismic (Fig. 2a) and geodetic (Fig. 2b) instruments installed offshore and onshore as a part of the 2016–2021 international collaborative research project Hazard Assessment of Large Earthquakes and Tsunamis in the Mexican Pacific Coast for Disaster Mitigation funded by the Japanese and Mexican governments through different agencies and institutions. Results from this collaboration should significantly contribute to risk mitigation in Mexico and to the identification of similarities (and differences) between the subduction zones of Japan and Mexico, leading to a better understanding of the physical mechanisms of megathrust earthquakes and tsunamis in subduction margins.

SEISMOGEODETIC AMPHIBIOUS NETWORK

Our observational network consists of seismometers and geodetic instruments without telemetry that have been installed both offshore and onshore around the GGap. The set of seismological stations (Fig. 2a) consists of 15 broadband seismometers (red and purple triangles) and 7 ocean-bottom seismometers (OBSs) (pink triangles). There are three different types of geodetic stations (Fig. 2b). Onshore, the network consists of 33 Global Positioning System (GPS) stations (red, blue, and black circles). Offshore, it consists of 7 ocean-bottom pressure gauges (OBPs) (yellow triangles) and 2 GPS-acoustic (GPS-A) sites (pink circles). Figure 3 shows some of the instruments and installation infrastructure of the network. It is worth mentioning that, to our knowledge, this is the first deployment of OBP and GPS-A stations in Mexico and Central America. Each GPS-A site is composed of three ocean-bottom transponders describing a triangle, as shown in Figure 4, in which we present an overview of the whole submarine network. Because the whole network was installed in 2017, we do not have enough data yet to pursue scientific goals. However, initial data-recovery efforts have allowed us to verify the good performance of several sites. Figure 5 shows, for instance, the first ocean-bottom pressure records with sampling rate of 30 min obtained a few days after the deployment of the two OBP stations collocated with the GPS-A sites (yellow triangles within pink circles in Fig. 2b). Daily tide effects nicely correlate in both sites, although they lie at very different depths (i.e., mean pressure values are 99.99 and 240.02 bar at OBPs 2305 and 2306, respectively). The most prominent data gap at station 2306 in 17 November was caused by station configuration difficulties that were solved.

To perform GPS-A measurements, we acquired an autonomous Wave Glider (WG) vehicle (Fig. 3b,d) equipped with cutting-edge instrumentation composed of two differential GPS antennas, an optical fiber gyroscope, an acoustic transducer, a control unit, and solar panels based on a design by the University of Singapore (Sylvain Barbot, personal comm., 2017) and Seatronics Co., following the concept from University of California San Diego (Spiess *et al.*, 1998; Chadwell and Spiess, 2008; David Chadwell, personal comm., 2016). To determine the geographic position of the ocean-bottom transponders array of each GPS-A site, the WG communicates acoustically with each transponder while determining the exact position of its transducer by means of both GPS antennas and the gyroscope. To avoid interference of the two-way traveling acoustic signals, we configured the transponders so that they respond to the WG pings with a precise differential delay. The vehicle makes a circular path of 100-m radius above the center of the array during the whole observational period (i.e., 12 hrs of continuous measurements), so the transponder answering delays were set considering the periodic time delays associated with the WG circular path. Figure 6 shows the travel times per transponder obtained in the deepest GPS-A site (2400 m depth, Figs. 2b and 3) during the first 12-hr observational period. Many different configuration tests via satellite communication were done in the WG unit control and transponders until we managed to find the right setup (around

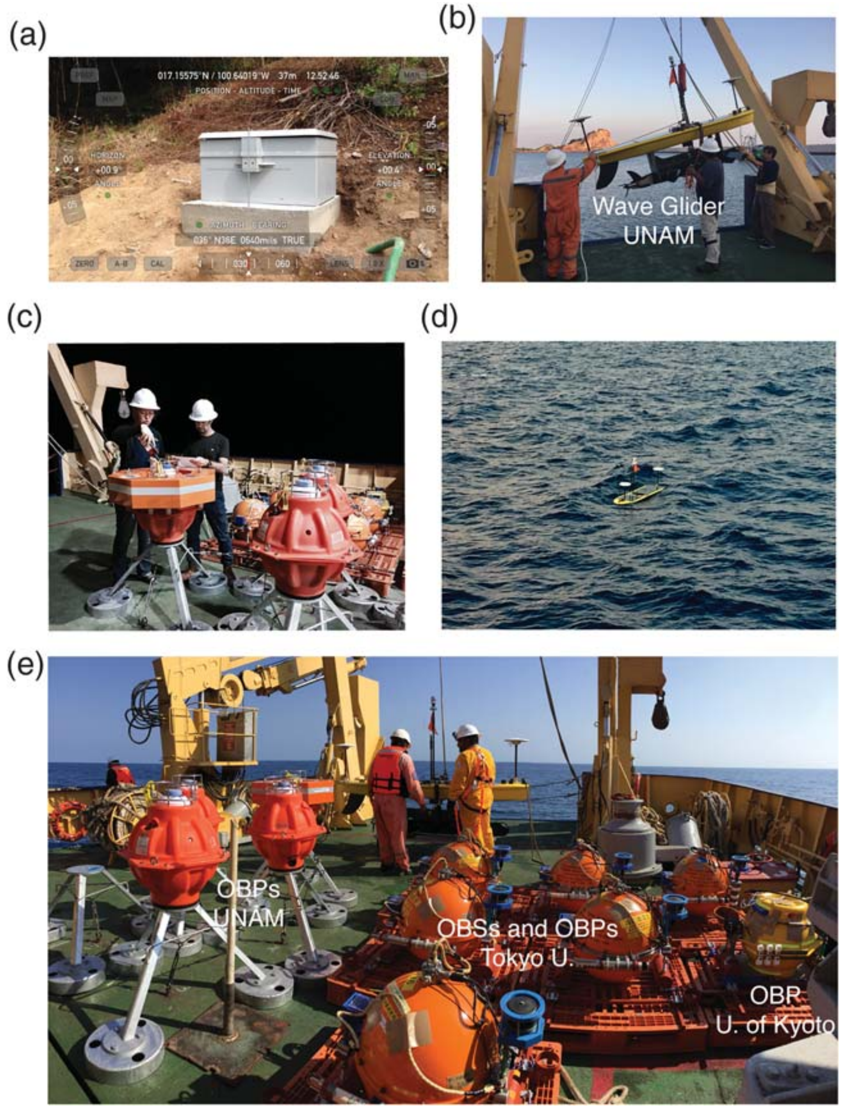

▲ **Figure 3.** Some instruments and infrastructure of the seismogeodetic network. (a) Typical steal case with concrete base and 1.5-m-deep borehole (not shown) used for the installation of onshore broadband seismometers, (b) deployment of the Wave Glider vehicle from the R/V *El Puma* of UNAM, (c) acoustic configuration of deep-water OBPs, (d) operation of the Wave Glider in open ocean, and (e) different ocean-bottom instruments in the R/V *El Puma* during the network deployment in November 2017.

▲ **Figure 4.** Schematic illustrating the ocean-bottom instruments deployed in the GGap, which consists of seven OBSs, seven OBPs, and two GPS-A sites (see Table 1 for details). Notice that each GPS-A site is composed of an array of three transponders. In the surface, we illustrate both the R/V *El Puma* and the Wave Glider used for the GPS-A measurements.

05:00 a.m. in the figure). About 7000 individual measurements were obtained in each GPS-A site that are now being processed to determine their geographical positions with an expected uncertainty smaller than 5 cm (Kido *et al.*, 2006).

Figure 7a shows the north–south GPS displacements recorded in eight stations from our onshore network during the past two years (see Fig. 2b for the stations location). There we can see the crustal elastic rebound caused by the occurrence of an SSE in 2017, characterized by southward displacements (i.e., negative slopes that reveal trenchward movement) in all stations. The 19 September 2017 M_w 7.1 intermediate-depth earthquake, which caused large damage in Mexico City, is indicated in the figure (dashed line), in which we clearly see the coseismic displacement in at least five stations up to a distance 180 km away from the epicenter (i.e., up to DOAR station, see Fig. 2b). To better estimate the duration of the SSE (Fig. 7b), displacements at stations CAYA, ARIG, and YAIG were detrended by removing the secular inter-SSE strain field (Kostoglodov *et al.*, 2003) and then averaged (gray line) and fitted with a sigmoid function (purple curb). The average displacement field reveals the occurrence of a 6-month-long SSE in Guerrero beginning in May and ending in October 2017. Compared with previous SSEs in the region (e.g., Radiguet *et al.*, 2012), this ~2.2 cm signal suggests that the 2017 SSE event is significantly smaller. GPS data from the rest of the stations are now being recovered in the field and processed to invert applying the method described in the Slow-Slip and Seismic Coupling Resolution section in terms of slip on the plate interface.

Figure 8 shows the north–south velocity seismograms recorded in four broadband stations of the network (Fig. 2a) for the 19 September M_w 7.1 intraslab earthquake. Since the event occurred only 120 km south of the city and 57 km below the boundaries of the Morelos and Puebla states, induced velocities saturated most of the seismometers. Records of smaller events in the region, including aftershocks of that earthquake, will allow us to image the crustal structure using different tomographic techniques (see the Crustal Tomography Resolution section) and study the seismotectonics of the region.

Deployment and operation of the offshore instruments are being conducted using the UNAM research vessel *El Puma*. The seismogeodetic amphibious network instruments specifications are given in Table 1. Scientists involved in the Mexico–Japan

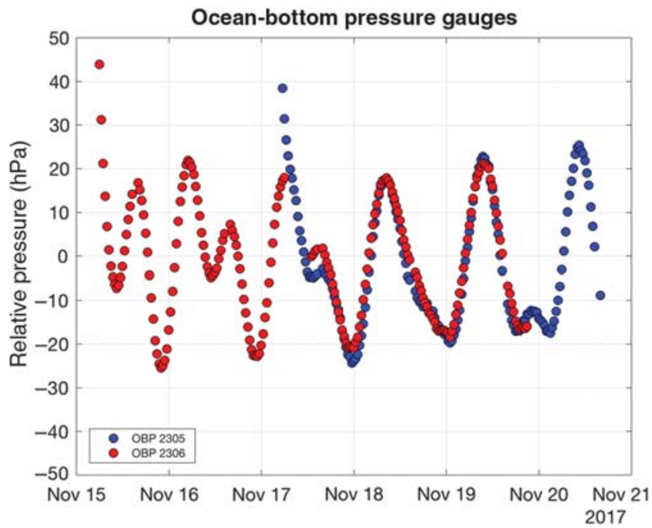

▲ **Figure 5.** First ocean-bottom pressure records obtained in the two OBP stations collocated with the GPS-A sites. Station depths are 1000 and 2400 m for 2305 and 2306 OBPs, respectively. Variations of ~40 hPa correspond to sea level changes caused by daily tides of ~40 cm.

collaborative project will analyze data from this network. Only 5 yrs after the end of the project (i.e., from March 2026), the data will be opened to the international community. The whole data set is being preprocessed and stored in a database at UNAM that is replicated in the University of Kyoto.

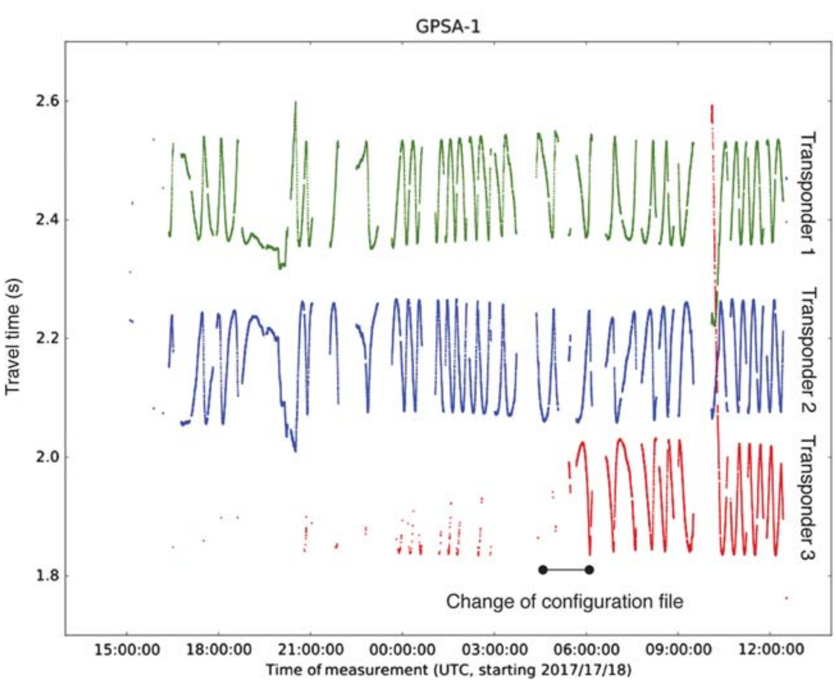

▲ **Figure 6.** Travel times of acoustic signals recorded using the Wave Glider via satellite communication for each one of the three ocean-bottom transponders composing the 2400-m-depth GPS-A site. See the Seismogeodetic Amphibious Network section for details.

Our observational network in Guerrero is complemented by three permanent networks belonging to UNAM and the Centro de Instrumentación y Registro Sísmico (CIRES). From UNAM, one belongs to the Servicio Sismológico Nacional (SSN) and consists of 10 observatories, each equipped with a Trimble GPS station, a STS-2 broadband seismometer, and a force-balance seismic sensor (FBA)-23 accelerometer (black triangles and circles in Fig. 2a,b, respectively). The other belongs to the Institute of Engineering, with 35 Kinemetrics FBA-23 accelerometers (green squares in Fig. 2a). From CIRES, the infrastructure consists of 42 strong-motion 23-bit stations (yellow circles in Fig. 2a). In total, the GGap and nearby regions (i.e., a region of ~400 km along the coast and ~250 km in the trench-perpendicular direction) are instrumented with 31 seismometers (most of them broadband), 48 geodetic stations, and 83 accelerometers. Data access from these three permanent networks is a prerogative belonging to the institutions in charge. However, broadband continuous data from the SSN are currently opened to the world upon request.

Seismogeodetic amphibious networks have only been deployed recently in a few regions of the globe such as Japan, New Zealand, Turkey, Chile, and the United States, producing unprecedented observations leading to a much deeper understanding of the plate-interface processes (e.g., Kanazawa *et al.*, 2009; Toomey *et al.*, 2014; Yamashita *et al.*, 2015; Wallace *et al.*, 2016). As discussed in the next section, our network design responds to the current knowledge we have of the seismotectonic activity in the GGap and surrounding regions and represents the best achievable compromise between resolution of future scientific studies and practical constrains imposed by inaccessible regions. Deployment of the network was completed in November 2017. Data from the network will allow pursuing different scientific goals for which the network has been designed in the framework of our Mexico–Japan collaboration, which involves about 73 researchers and 27 students from both countries. Among these goals are the (1) detection and imaging of any aseismic deformation processes in the plate interface; (2) mapping the temporal evolution of the seismic coupling; (3) generating reliable earthquake and tsunami scenarios for hazard assessment; (4) detection and analysis of slow, repeating, tsunami, and/or conventional earthquakes; (5) different seismotectonic studies; (6) determination of the crustal structure through tomographic studies using double-difference arrival times, regional events, and correlation of seismic noise; (7) detection and analysis of temporal variations of the crustal properties from noise correlations; and (8) receiver functions analysis. In case a large earthquake takes place in the region, the data will also be valuable for imaging the rupture process from local or regional strong-motion records and the static-strain field.

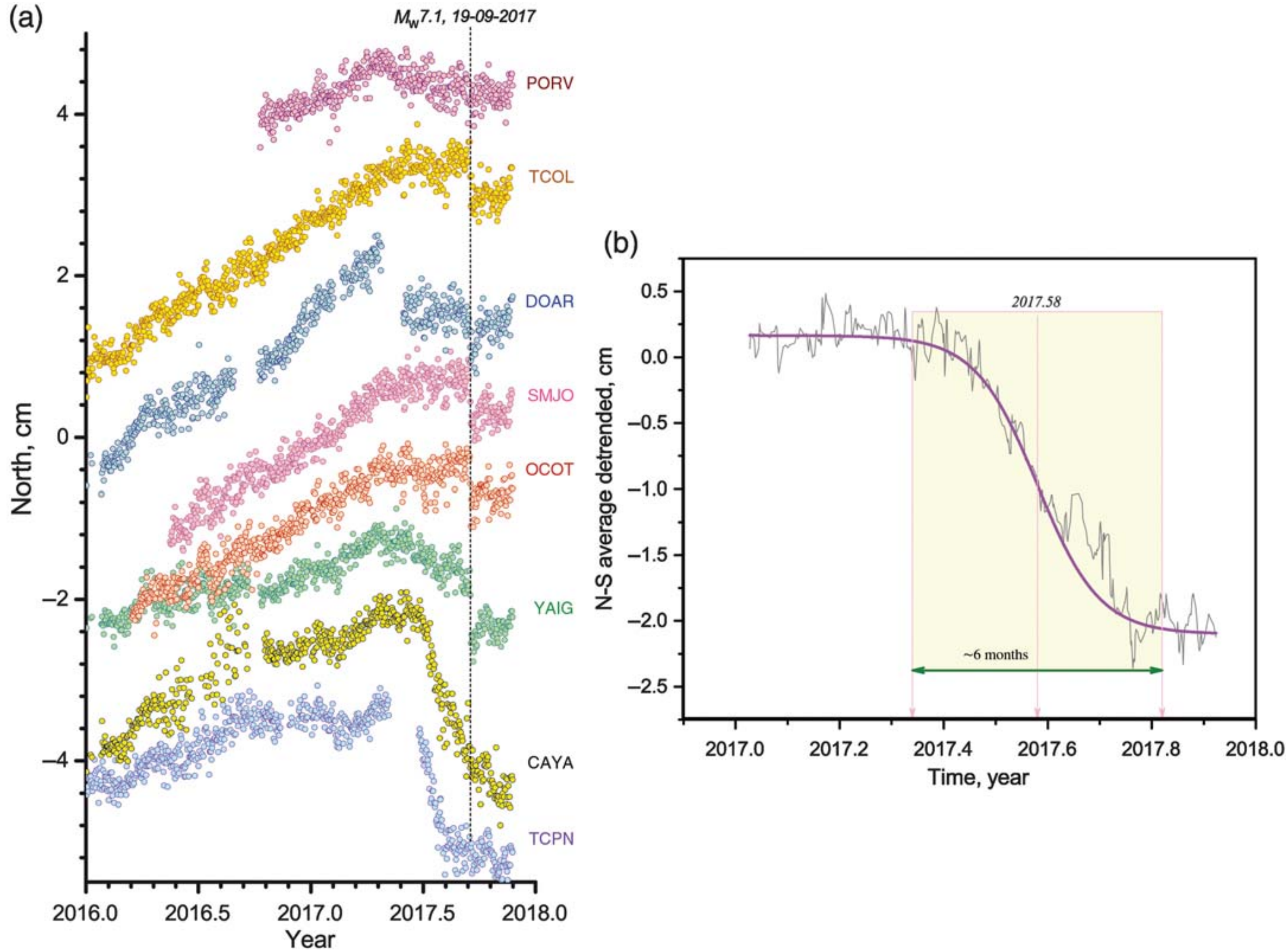

▲ **Figure 7.** North–south GPS displacements recorded in some of the onshore geodetic stations (locations of the stations are shown in Fig. 3). (a) Secular and the 2017 slow-slip event (SSE) displacements. The dashed line indicates the date of the 19 September M_w 7.1 earthquake that caused serious damage in Mexico City. (b) Detrended and averaged displacements (gray curve) from stations YAIG, ARIG, and CAYA fitted with the sigmoid function (purple) in which we estimated a duration of 6 months for the 2017 Guerrero SSE.

RESOLUTION OF THE OBSERVATIONAL NETWORK

The data provided by the observational network will allow for addressing a diversity of scientific problems. Relevance of a given geophysical network relies on its capability of answering specific questions. To quantify the scientific potential of our network, in this section, we present resolution tests considering the final instruments configuration for two methodological strategies that are essential to achieve important scientific and disaster prevention goals. Results from similar tests helped us to decide the best locations for the seismic and geodetic sites to maximize the resolvability of both tomographic and SSE/coupling imaging (e.g., thanks to those tests, we concluded that several coast-parallel lines of geodetic instruments with ~20 km separation were necessary to resolve the penetration of SSEs into the seismogenic segment of the megathrust). The tests also give us an idea of the characteristic lengths that will theoretically be resolved when the data are available, which are significantly smaller than those achieved in the region from previous investigations (e.g., Iglesias *et al.*, 2010; Radiguet *et al.*, 2012, 2016).

Crustal Tomography Resolution

Determining the continental and oceanic crustal structures from the trench to inland regions of Guerrero is essential to characterize both seismicity and the associated hazard. For instance, a well-resolved structure allows reliable scenario-earthquake simulations to quantify the ground motion in vulnerable population centers. The network provides the opportunity to generate tomographic images with unprecedented resolution. Here, we present resolution tests for two different imaging techniques that will be used to interpret the data from the network. Method 1 is based on double differences of relative and absolute arrival times from passive sources, and method 2 is based on dispersion

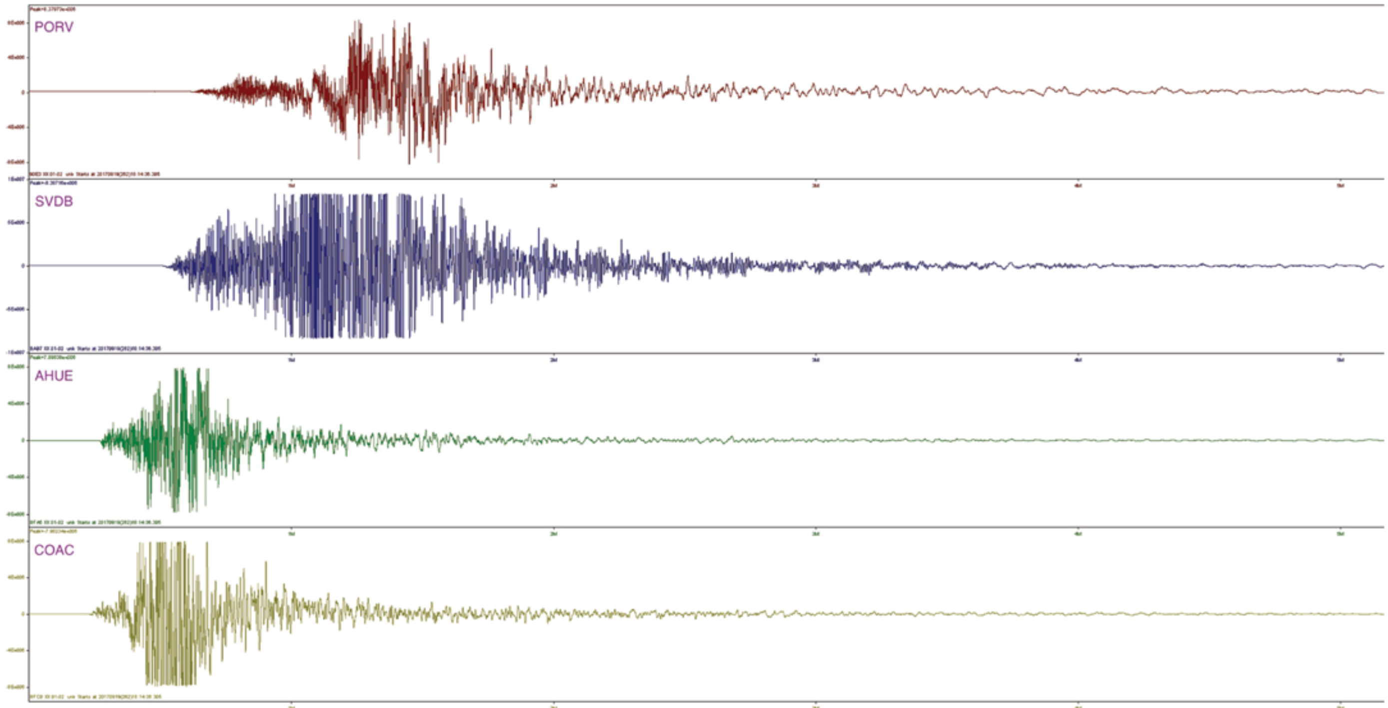

▲ **Figure 8.** North–south velocity seismograms recorded at four broadband stations of the onshore network for the 19 September M_w 7.1 earthquake that caused serious damage in Mexico City.

curves determined from the correlation of ambient noise and regional earthquakes.

Method 1: Seismic tomography based on the double-difference method (Zhang and Thurber, 2003). The algorithm determines 3D velocity models of V_P and V_S jointly, combining the absolute and relative event locations. This approach has the advantage of integrating relative arrival times between pairs of events with error estimates along with absolute arrival times, thereby retaining valuable information often dismissed when only adjusted picks are considered. The final models may be

Table 1
Technical Specifications of the Equipment Composing the Seismogeodetic Amphibious Network in the Guerrero Seismic Gap (GGap) Provided by the Mexico–Japan Collaborative Project

Onshore	Offshore
Seismic	
14 seismological stations consisting of:	7 ocean-bottom seismometers (OBS) consisting of:
1 Kinemetrics STS-2.5 sensor with Quanterra Q330S digitizer	7 Katsujima 1-Hz 3D sensors with HDDR-5 digitizer, and Tokyo Sokushin 1-Hz 3D digitizer with TOBS-24N
6 RefTek 151B-120 sensors with 6 RefTek 130-01 digitizers	
5 Güralp CMG-40T and 2 RefTek 151-60 sensors with 7 RefTek 130-01 digitizers	
Geodetic	
33 Global Positioning System (GPS) stations consisting of:	7 ocean-bottom pressure gauges (OBP) consisting of:
11 Zephyr 2 and 3 geodetic antennas, and Trimble NetR9 receivers	4 Sonardyne FETCH with Paroscientific pressure sensor (3000 and 6000 m)
22 Leica AT504 and Trimble Zephyr 2 geodetic antennas, and Trimble NetR9, Leica GRX1200 receivers	3 OBPs Paroscientific Inc., 8B4000-2-005, with data logger, Hakusan LS-9150
	2 GPS-acoustic (GPS-A) stations consisting of:
	4 Sonardyne FETCH without pressure sensor (3000 and 6000 m)

refined by applying the weighted average model method (Calò *et al.*, 2012, 2013), which is a postprocessing technique useful for any tomographic inversion method to overcome some limitations of the velocity models yielded by standard tomographic codes. The postprocessing method is based on sampling models compatible with data sets using different input parameters. New and more reliable models are then achieved by means of weighting functions based on the ray density (derivative weight sum; Toomey and Foulger, 1989).

To assess the minimum resolution lengths of the tomographic model, we set up a checkerboard test using a plausible earthquakes distribution expected to be recorded in the network during the next three years. We used the catalog of events reported by the SSN since 2000, assuming that the event rates and locations will not significantly change in the near future. We considered only events with $M_w > 3.9$ and declustered the catalog to remove seismic sequences leading to anomalous earthquake concentrations. Then we randomly selected the hypocenters to obtain a representative distribution of the foci with 442 events in a 3-yr lag time (Fig. 9). For the test, we assumed that at least 80% of the seismic stations would record the events. We considered 29 stations, from which the international project supplied 21 and the rest belong to the SSN. To make our resolution tests even more conservative, we did not to include the strong-motion stations from the Institute of Engineering and the Sistema de Alerta Sísmica Mexicano (SASMEX) belonging to the Centro de Instrumentación y Registro Sísmico (CIRES) (green and yellow symbols in Fig. 2a).

The checkerboard model is characterized by alternating positive and negative velocity changes of $\pm 5\%$ with respect to the initial 1D velocity model. Each patch has a size of $20 \times 20 \times 10$ km^3 in the X, Y, and Z directions, respectively. This model was then used to calculate synthetic travel times using the selected earthquake locations and stations. Possible travel-time errors were integrated by adding Gaussian distributed noise with standard deviations of 0.02 and 0.04 s to the P and S travel times, respectively, which correspond to the largest expected picking error for local or regional data sets digitalized at 100 samples per second (Chiarabba and Moretti, 2006). Figure 9 shows the resulting model from the inversion, in which we conclude that the crustal and the upper mantle structures are well resolved in a large region surrounding the GGap at least for velocity anomalies with characteristic lengths similar to the dimensions of the checkerboard patches tested here (20 km horizontally and 10 km vertically).

Method 2: Seismic tomography based on surface-wave dispersion curves obtained from noise cross correlations of pairs of stations. To obtain dispersion curves, we follow the standard procedure proposed by Bensen *et al.* (2007). Data from pairs of inland broadband stations (BB–BB) provide dispersion curves from ~1 to 50 s depending on the interstation distances (e.g., Spica *et al.*, 2014).

Dispersion curves can be computed for pairs of stations offshore (OBS–OBS) and combinations onshore–offshore sites (BB–OBS) that are expected to have a limited bandwidth between ~1 and ~10 s given the short-period flat response of the OBSs. In addition, dispersion curves can also be computed for local and regional earthquakes recorded in the network. This mixed data set not only contributes to improving the resolution of tomographic images but also to obtain tomographic images for longer periods (> 10 s). Individual dispersion curves for each pair of station–station and/or earthquake–station can be inverted in a tomographic sense using the fast-marching method developed by Rawlinson and Sambridge (2005). See Iglesias *et al.* (2010) and Spica *et al.* (2014) for details.

To assess the nominal resolution of tomographic images considering only noise correlation between pairs of stations close to the coast, we performed a checkerboard test assuming that it is possible to obtain velocity group measurements for some period between all stations. This hypothesis is only valid for wavelengths smaller than the interstation distances. Of course, for period longer than those distances, the tomographic resolution would be lower. The study area was subdivided into 20×20 cells of 0.1° (~11 km). For the checkerboard test, cells are set with alternating positive and negative velocity changes of $\pm 8\%$ with respect to a reference initial homogeneous model (2.6 km/s). Figure 10 shows the results from the synthetic inversion using the checkerboard model. The inversion scheme recovers, reasonably well, the target configuration for the area surrounded by the stations up to distances smaller than 5 km from the trench (not shown).

Slow-Slip and Seismic Coupling Resolution

The evolution of both slow-slip transients and the seismic coupling in Guerrero has critical implications in the mechanics of the plate interface and the seismic hazard. Observations from our geodetic amphibious network will lead to unprecedented results in these matters across the state of Guerrero by making possible reliable estimates of the seismic potential leading to realistic earthquake scenarios, for instance. In this section, we assess the nominal resolution for the slip (or back-slip) inversion in a constrained optimization framework using the adjoint method for a simple and efficient gradient evaluation of the cost function (Tarantola, 1984; Plessix, 2006). The hypothetical observations correspond to displacement time series recorded at onshore GPS stations and offshore OBP and GPS-A sites of our geodetic network. From a linear formulation of the elastostatic problem and a quadratic cost function given by the square difference of the observed and synthetic displacements, the resulting optimization problem is convex and has a unique solution. Two of the most valuable advantages of this optimization strategy are (1) that the slip function in the plate interface is not parameterized and (2) that it is possible to estimate, *a posteriori*, the formal uncertainty of the model parameters. The lack of complete fault illumination, the noise in the data, and the model uncertainties hamper the slip or coupling inversions. Regularization and prior model terms can be integrated in the problem formulation for overcoming these problems to some extent. However, here we present a simple exercise excluding noise and model uncertainties that allows us to assess the benefit of our improved geodetic

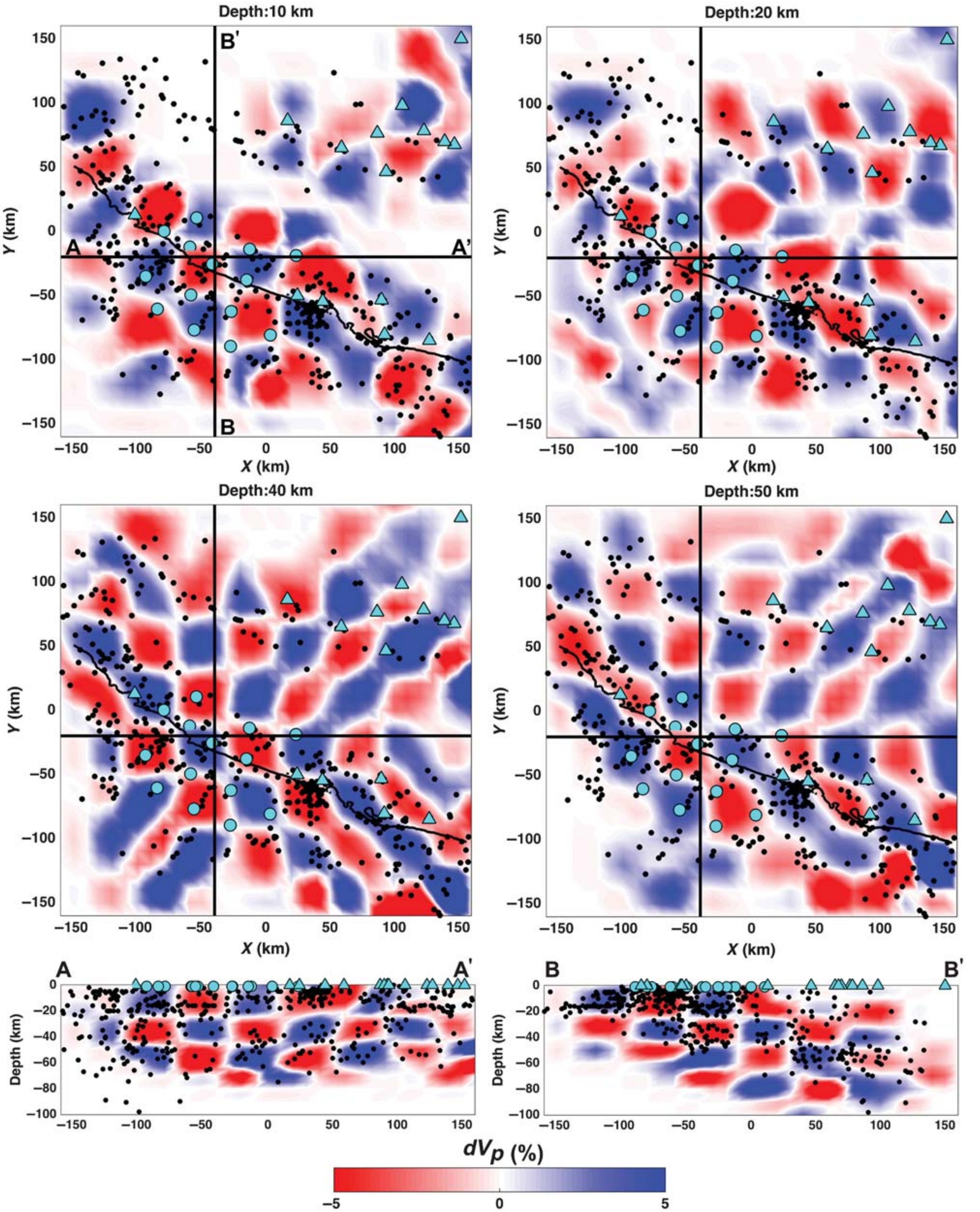

▲ **Figure 9.** Checkerboard resolution test for double-difference travel-time tomography. The checkerboard velocity cells are 20 × 20 km length horizontally and 10 km in depth. See the Crustal Tomography Resolution section for details.

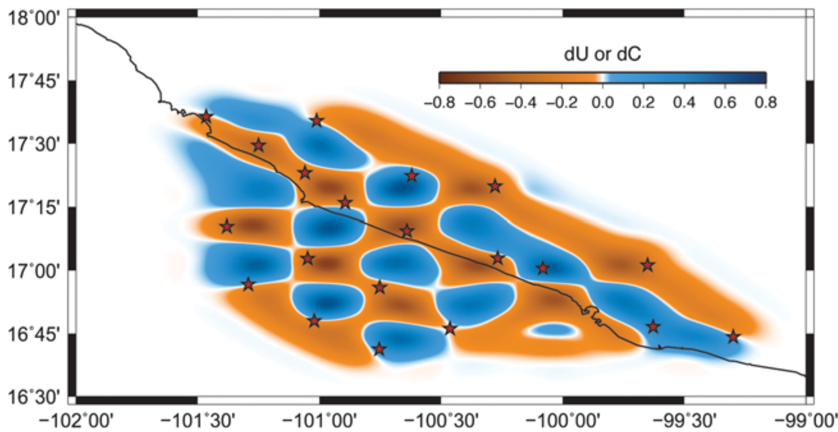

▲ **Figure 10.** Checkerboard resolution test assuming that it is possible to obtain travel times (corresponding to phase C or group U velocities) between all pairs of stations from the cross correlation of seismic noise. The checkerboard velocity cells are 0.1° (~11 km) per side.

network compared with the preceding instrumentation in the region.

We performed a series of synthetic inversion tests considering the actual observational network, a homogeneous full space, and the 3D plate-interface geometry used by Radiguet *et al.* (2016). The interface is discretized by subfaults with horizontal square projections of 5 km per side. Figure 11a shows the result for a checkerboard inversion test in which only the along-dip-slip component was inverted. Please notice the almost perfect fit between the data and the model predictions. The checkerboard is composed of squares with 80 km per side and slip of either 0 or 30 cm in the along-dip direction. Although smoother, slip-imaging results obtained when also inverting the along-strike component are very similar (not shown). For most of the sites offshore, we only inverted the vertical displacement component, which is being recorded by the OBPs, but for the two GPS-A sites, the three components were inverted. It is remarkable how well the checkerboard pattern is resolved in a huge area (e.g., inside the black contour in which the slip was larger than 5 cm during the 2006 SSE after Cavalié *et al.*, 2013) despite the fine discretization of the source (i.e., the small size of subfaults) and the absence of problem regularization to stabilize the inversion. In particular, we conclude that the slip offshore can only be resolved beyond ~20 km from the coast where ocean-bottom instruments are deployed.

To illustrate the benefit of the improved geodetic network for imaging SSEs or plate coupling, we inverted a Gaussian slip distribution (target model shown in Fig. 11b) excluding (Fig. 11c) and including (Fig. 11d) the geodetic instruments provided by the government of Japan. The target model was chosen to resemble the slip distribution determined by Cavalié *et al.* (2013) for the 2006 SSE (i.e., most of the slip is embedded within the black contour). The tests clearly show that the new observational network substantially improves the slip reconstruction not only between 20- and 40-km depth but also below the coast and the adjacent offshore region, where we find a significant overestimation of the slip in the absence of marine stations and a dense GPS array (Fig. 11c). This region is of special interest because we do not know whether offshore slow slip plays a major role during the seismic cycle.

CONCLUSIONS AND PERSPECTIVES

Thanks to a major collaborative effort between Mexican and Japanese scientists, we have instrumented in 2017 the GGap and neighboring regions with the first seismogeodetic amphibious network in Mexico and Central America. This gap probably represents the largest natural threat to large populated areas such as Mexico City, with more than 22 million people, which may experience ground motions significantly larger than those felt during the disastrous 1985 Michoacan earthquake if the gap breaks in a similar or larger event. In that scenario, important coastal population centers such as Acapulco and Ixtapa-Zihuatanejo, among others, could also experience overwhelming ground shaking and tsunamis.

The observational network is generating unprecedented data in the region, which is expected to deepen our understanding of the subduction process and to provide more reliable estimates of the seismic and tsunami hazards along the Pacific coast of Mexico. We presented initial data recorded in our seismogeodetic amphibious network, in which we reported the occurrence of a 6-month-long SSE in Guerrero (i.e., from May to October 2017) and the ground motion induced by the devastating 19 September 2017 M_w 7.1 earthquake. We also reported the first offshore geodetic measurements ever recorded in Mexico and Central America using OBPs and GPS-A stations. To assess the benefit of the new observational network, we quantified its resolution through nominal tests for both the crustal and plate-interface slip imaging. These tests were also conducted prior to the instruments' deployment for network design purposes. The presented results show that the network should lead to earth models resolving structural features with characteristic lengths of at least 20 and 10 km in the horizontal and vertical directions, respectively, across the state of Guerrero in the crust and upper mantle. Similarly, onshore and offshore geodetic instruments should lead to unprecedented images up to the trench of the seismic coupling and slow slip in the plate interface. We showed that the previous instrumentation in the region was insufficient for reliably imaging the SSEs below the coast and offshore across the GGap.

For mitigating the risk associated with the GGap, researchers of the binational collaboration are developing sophisticated physics-based models to simulate hypothetical scenario earthquakes in the gap and the associated tsunamis with realistic inundations. These models are being constrained by observations from the observational network that, as shown in this

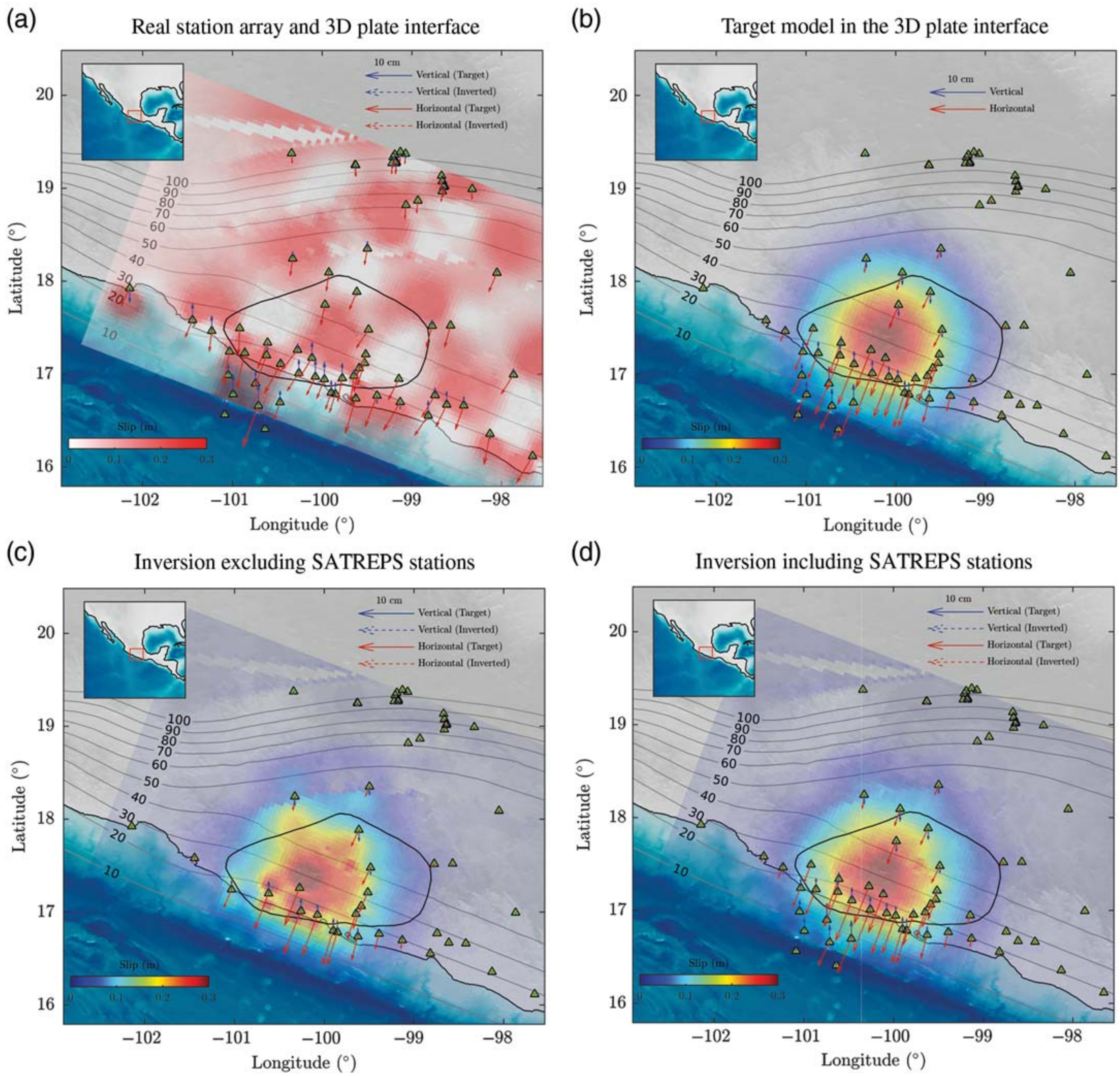

▲ **Figure 11.** Synthetic inversion tests using a recently developed adjoint inverse method for imaging SSEs and the seismic coupling in the 3D plate interface (gray contours). (a) Result from a checkerboard test considering all stations of the geodetic amphibious network. (c) and (d) show the inversion results excluding and including the geodetic stations provided by the Japanese government, respectively, for the Gaussian-slip distribution shown in (b) (i.e., target model). The black contour depicts the 5-cm slip contour determined by Cavalié *et al.* (2013) for the 2006 SSE in Guerrero.

article, will benefit from high-resolution analyses of the crustal structure and the seismic coupling in the plate interface. Furthermore, risk management and educational experts from both countries are developing risk mitigation guidelines along with local authorities of civil protection and school teachers that are being implemented in this moment. This multidisciplinary effort is now translating data from the observational network into specific measures or strategies for reducing the risk of the population facing the possibility of a major earthquake or tsunami in the GGap. As the project progresses in the next few years, detailed hazard assessments along the coast will be delivered to different experts and institutions for raising awareness and designing end-to-end risk mitigation recommendations in highly exposed localities.

DATA AND RESOURCES

The data reported in this study were recorded in our seismogeodetic network except for the Global Positioning System (GPS) records at stations YAIG and ARIG, which belong to the Servicio Sismologico Nacional (SSN) of National Autonomous University of Mexico (UNAM) (www.ssn.unam.mx, last accessed April 2018). The data generated by the seismogeodetic network will be available for the scientific community until 2026 through personal request to V. M. C. and Y. I. Some plots were made using the Generic Mapping Tools v. 4.2.1 (www.soest.hawaii.edu/gmt, last accessed April 2018; Wessel and Smith, 1998) and the MATLAB software v. R2017a (www.mathworks.com, last accessed April 2018). The unpublished manuscript by V. M. Cruz-Atienza, C. D. Villafuerte, and H. S. Bhat (2018), "Rapid tremor migration and pore-pressure waves in subduction zones," accepted in *Nature Communications*.

ACKNOWLEDGMENTS

The seismogeodetic amphibious network and the associated binational research project is being funded by (1) the Japanese government through the program Science and Technology Research Partnership for Sustainable Development (SATREPS) via the Japan International Cooperation Agency (JICA) and the Japan Science and Technology Agency (JST) and through the Universities of Kyoto (U of K) and Tokyo with Grant Number 15543611 and MEXT KAKANHI Number 16H02219, respectively, and (2) the Mexican government through the Universidad Nacional Autónoma de México (UNAM) with PAPIIT Grant Numbers IN113814, IN111316, IG100617, IN115613, and IN107116, its Coordinación de la Investigación Científica (CTIC and COPO) with research vessel time, its central administration through importation fees, its Instituto de Ciencias del Mar y Limnología - Unidad Mazatlán, and its Servicio Sismológico Nacional (SSN); the Consejo Nacional de Ciencia y Tecnología (CONACyT) through Grant Numbers 268119, 273832, and 255308; the Mexican Ministry of Foreign Affairs through the Agencia Mexicana de Cooperación Internacional para el Desarrollo (AMEXCID); and the Centro Nacional de Prevención de Desastres (CENAPRED). For their support and collaboration in the acquisition of the GPS-A measurements, the authors especially thank Sharadha Sathiakumar, Grace Chia, Sylvain Bar- bot, and David Chadwell. The authors specially thank the outstanding work of Arika Nagata, Kumiko Ogura, Vanessa Ayala, Liliana Córdova, José Luis Carballo, Lorena García, José Antonio Santiago, Ekaterina Kazachkina, and Sara Ivonne Franco, as well as all the administrative staffs from the U of K, UNAM, JICA, JST, AMEXCID, and CONACyT that made all this possible. The authors also especially thank the Secretaría de Protección Civil del Estado de Guerrero and the Secretaría de Marina (SEMAR) for their unconditional support.

REFERENCES

Anderson, J. G., P. Bodin, J. N. Brune, J. Prince, S. K. Singh, R. Quaas, and M. Onate (1986). Strong ground motion from the Michoacan, Mexico, earthquake, *Science* **233,** 1043–1049.

Bartlow, N. M., N. M. Bartlow, S. Miyazaki, S. Miyazaki, A. M. Bradley, A. M. Bradley, P. Segall, and P. Segall (2011). Space-time correlation of slip and tremor during the 2009 Cascadia slow slip event, *Geophys. Res. Lett.* **38,** L18309, doi: 10.1029/2011GL048714.

Bensen, G. D., M. H. Ritzwoller, M. P. Barmin, A. L. Levshin, F. Lin, M. P. Moschetti, N. M. Shapiro, and Y. Yang (2007). Processing seismic ambient noise data to obtain reliable broad band surface wave dispersion measurements, *Geophys. J. Int.* **169,** 1239–1260, doi: 10.1111/j.1365-246X.2007.03374.x.

Calò, M., C. Dorbath, D. Luzio, S. G. Rotolo, and G. D'Anna (2012). Seismic velocity structures of southern Italy from tomographic imaging of the Ionian slab and petrological inferences, *Geophys. J. Int.* **191,** no. 2, 751–764, doi: 10.1111/j.1365-246X.2012.05647.x.

Calò, M., L. Parisi, and D. Luzio (2013). Lithospheric *P* and *S* wave velocity models of the Sicilian area using WAM tomography: Procedure and assessments, *Geophys. J. Int.* doi: 10.1093/gji/ggt252.

Cavalié, O., E. Pathier, M. Radiguet, M. Vergnolle, N. Cotte, A. Walpersdorf, V. Kos-toglodov, and F. Cotton (2013). Slow slip event in the Mexican subduction zone: Evidence of shallower slip in the Guerrero seismic gap for the 2006 event revealed by the joint inversion of InSAR and GPS data, *Earth Planet. Sci. Lett.* **367,** 52–60, doi: 10.1016/j.epsl.2013.02.020.

Chadwell, C. D., and F. N. Spiess (2008). Plate motion at the ridge-transform boundary of the south Cleft segment of the Juan de Fuca Ridge from GPS-acoustic data, *J. Geophys. Res.* **113,** no. B04415, doi: 10.1029/2007jb004936.

Chiarabba, C., and M. Moretti (2006). An insight into the unrest phenomena at the Campi Flegrei caldera from V_P and V_P/V_S tomography, *Terra Nova* **18,** no. 6, 373–379.

Cotte, N., A. Walpersdorf, V. Kostoglodov, M. Vergnolle, J. Santiago, I. Manighetti, and M. Campillo (2009). Anticipating the next large silent earthquake in Mexico, *Eos Trans. AGU* **90,** no. 21, 181–182.

Cruz-Atienza, V. M., A. Husker, D. Legrand, E. Caballero, and V. Kostoglodov (2015). Nonvolcanic tremor locations and mechanisms in Guerrero, Mexico, from energy-based and particle motion polarization analysis, *J. Geophys. Res.* **120,** 275–289, doi: 10.1002/2014JB011389.

Duke, C. M., and D. J. Leeds (1959). Soil conditions and damage in the Mexico earthquake of July 28, 1957, *Bull. Seismol Soc. Am.* **49,** no. 2, 179–191.

Frank, W. B., N. M. Shapiro, A. L. Husker, V. Kostoglodov, A. Romanenko, and M. Campillo (2014). Using systematically characterized low-frequency earthquakes as a fault probe in Guerrero, Mexico, *J. Geophys. Res.* **119,** doi: 10.1002/2014JB011457.

Hirose, H., and K. Obara (2010). Recurrence behavior of short-term slow slip and correlated nonvolcanic tremor episodes in western Shikoku, southwest Japan, *J. Geophys. Res.* **115,** no. B00A21, doi: 10.1029/2008JB006050.

Husker, A. L., V. Kostoglodov, V. M. Cruz-Atienza, D. Legrand, N. M. Shapiro, J. S. Payero, M. Campillo, and E. Huesca-Pérez (2012). Temporal variations of non-volcanic tremor (NVT) locations in the Mexican subduction zone: Finding the NVT sweet spot, *Geochem. Geophys. Geosys.* **13,** Q03011, doi: 10.1029/2011GC003916.

Iglesias, A., R. W. Clayton, X. Pérez-Campos, S. K. Singh, J. F. Pacheco, D. García, and C. Valdés-González (2010). *S* wave velocity structure below central Mexico using high-resolution surface wave tomography, *J. Geophys. Res.* **115,** no. B06307, doi: 10.1029/2009JB006332.

Ito, Y., R. Hino, M. Kido, H. Fujimoto, Y. Osada, D. Inazu, Y. Ohta, T. Iinuma, M. Ohzono, S. Miura, *et al.* (2013). Episodic slow slip events in the Japan subduction zone before the 2011 Tohoku-

Oki earthquake, *Tectonophysics* **600,** 14–26, doi: 10.1016/j.tecto.2012.08.022.
Ito, Y., R. Hino, S. Suzuki, and Y. Kaneda (2015). Episodic tremor and slip near the Japan trench prior to the 2011 Tohoku-Oki earthquake, *Geophys. Res. Lett.* **42,** 1725–1731, doi: 10.1002/2014GL062986.
Kanamori, H., P. C. Jennings, S. K. Singh, and L. Astiz (1993). Estimation of strong ground motions in Mexico city expected for large earthquakes in the guerrero seismic gap, *Bull. Seismol Soc. Am.* **83,** no. 3, 811–829.
Kanazawa, T., M. Shinohara, and H. Shiobara (2009). Recent progress in seafloor earthquake observations and Instruments in Japan, *Zisin* **2,** no. 61, S55–S68.
Kato, A., K. Obara, T. Igarashi, H. Tsuruoka, S. Nakagawa, and N. Hirata (2012). Propagation of slow slip leading up to the 2011 M_w 9.0 Tohoku-Oki earthquake, *Science* **335,** 705–708, doi: 10.1126/science.1215141.
Kido, M., H. Fujimoto, S. Miura, Y. Osada, K. Tsuka, and T. Tabei (2006). Seafloor displacement at Kumano-nada caused by the 2004 off Kii Peninsula earthquakes, detected through repeated GPS/Acoustic surveys, *Earth Planets Space* **58,** no. 7, 911–915, doi: 10.1186/BF03351996.
Kostoglodov, V., and J. F. Pacheco (1999). *Cien Años de Sismicidad en Mexico*, Poster, Instituto de Geofísica, Universidad Nacional Autónoma de México (in Spanish).
Kostoglodov, V., A. L. Husker, N. M. Shapiro, J. S. Payero, M. Campillo, N. Cotte, and R. W. Clayton (2010). The 2006 slow slip event and nonvolcanic tremor in the Mexican subduction zone, *Geophys. Res. Lett.* **37,** L24301, doi: 10.1029/2010GL045424.
Kostoglodov, V., S. Singh, J. Santiago, S. Franco, K. Larson, A. Lowry, and R. Bilham (2003). A large silent earthquake in the Guerrero seismic gap, Mexico, *Geophys. Res. Lett.* **30,** no. 15, 1807, doi: 10.1029/2003GL017219.
Lay, T., H. Kanamori, C. J. Ammon, K. D. Koper, A. R. Hutko, L. Ye, H. Yue, and T. M. Rushing (2012). Depth-varying rupture properties of subduction zone megathrust faults, *J. Geophys. Res.* **117,** no. B04311, doi: 10.1029/2011JB009133.
Maury, J., S. Ide, V. M. Cruz-Atienza, V. Kostoglodov, G. González-Molina, and X. Pérez-Campos (2016). Comparative study of tectonic tremor locations: Characterization of slow earthquakes in Guerrero, Mexico, *J. Geophys. Res.* **121,** 5136–5151, doi: 10.1002/2016JB013027.
National Autonomous University of Mexico (UNAM) Seismology Group (2015). Papanoa, Mexico, earthquake of 18 April 2014 (M_w 7.3), *Geofís. Int.* **54,** 363–386.
Núñez-Cornú, F. J., M. Ortiz, and J. J. Sánchez (2008). The great 1787 Mexican tsunami, *Nat. Hazards* **47,** 569–576, doi: 10.1007/s11069-008-9239-1.
Payero, J. S., V. Kostoglodov, N. Shapiro, T. Mikumo, A. Iglesias, X. Pérez-Campos, and R. W. Clayton (2008). Nonvolcanic tremor observed in the Mexican subduction zone, *Geophys. Res. Lett.* **35,** L07305, doi: 10.1029/2007GL032877.
Plessix, R. E. (2006). A review of the adjoint-state method for computing the gradient of a functional with geophysical applications, *Geophys. J. Int.* **167,** no. 2, 495–503.
Radiguet, M., F. Cotton, M. Vergnolle, M. Campillo, A. Walpersdorf, N. Cotte, and V. Kostoglodov (2012). Slow slip events and strain accumulation in the Guerrero gap, Mexico, *J. Geophys. Res.* **117,** no. B04305, doi: 10.1029/2011JB008801.
Radiguet, M., H. Perfettini, N. Cotte, A. Gualandi, B. Valette, V. Kostoglodov, T. Lhomme, A. Walpersdorf, E. Cabral Cano, and M. Campillo (2016). Triggering of the 2014 M_w 7.3 Papanoa earthquake by a slow slip event in Guerrero, Mexico, *Nature Geosci.* **9,** no. 11, 829–833, doi: 10.1038/ngeo2817.
Ramirez-Herrera, M. T., A. Cundy, V. Kostoglodov, A. Carranza-Edwards, E. Morales, and S. Metcalfe (2007). Sedimentary record of late-Holocene relative sea-level change and tectonic deformation from the Guerrero Seismic Gap, Mexican Pacific Coast, *The Holocene* **17,** no. 8, 1211–1220, doi: 10.1177/0959683607085127.
Rawlinson, N., and M. Sambridge (2005). The fast marching method: An effective tool for tomographic imaging and tracking multiple phases in complex layered media, *Explor. Geophys.* **36,** 341–350.
Ruiz, S., M. Metois, A. Fuenzalida, J. Ruiz, F. Leyton, R. Grandin, C. Vigny, R. Madariaga, and J. Campos (2014). Intense foreshocks and a slow slip event preceded the 2014 Iquique M_w 8.1 earthquake, *Science* **345,** no. 6201, doi: 10.1126/science.1256074.
Singh, S. K., L. Astiz, and J. Havskov (1981). Seismic gaps and recurrence periods of large earthquakes along the Mexican subduction zone: A reexamination, *Bull. Seismol. Soc. Am.* **71,** 827–843.
Singh, S. K., J. M. Espindola, J. Yamamoto, and J. Havskov (1982). Seismic potential of Acapulco-San Marcos region along the Mexican subduction zone, *Geophys. Res. Lett.* **9,** 633–636.
Spica, Z., V. M. Cruz-Atienza, G. Reyes-Alfaro, D. Legrand, and A. Iglesias-Mendoza (2014). Crustal imaging of western Michoacán and the Jalisco block, Mexico, from ambient seismic noise, *J. Volcanol. Geoth. Res.* **289,** 1–9, doi: 10.1016/j.jvolgeores.2014.11.005.
Spiess, F. N., C. D. Chadwell, J. A. Hildebrand, L. E. Young, J. G. H. Purcell, and H. Dragert (1998). Precise GPS/acoustic positioning of seafloor reference points for tectonic studies, *Phys. Earth Planet. In.* **108,** 101–112.
Suárez, G., and P. Albini (2009). Evidence for great tsunamigenic earthquakes (M 8.6) along the Mexican subduction zone, *Bull. Seismol. Soc. Am.* **99,** no. 2A, 892–896, doi: 10.1785/0120080201.
Tarantola, A. (1984). Inversion of seismic reflection data in the acoustic approximation, *Geophysics* **49,** no. 8, 1259–1266.
Toomey, D. R., and G. R. Foulger (1989). Tomography inversion of local earthquake data from the Hengill: Grensdalur central volcano complex, Iceland, *J. Geophys. Res.* **94,** 17,497–17,510.
Toomey, D. R., R. M. Allen, A. H. Barclay, S. W. Bell, P. D. Bromirski, R. L. Carlson, X. Chen, J. A. Collins, R. P. Dziak, B. Evers, *et al.* (2014). The Cascadia Initiative: A sea change in seismological studies of subduction zones, *Oceanography* **27,** no. 2, 138–150.
Villafuerte, C., and V. M. Cruz-Atienza (2017). Insights into the causal relationship between slow slip and tectonic tremor in Guerrero, Mexico, *J. Geophys. Res.* **122,** doi: 10.1002/2017JB014037.
Wallace, L. M., S. C. Webb, Y. Ito, K. Mochizuki, R. Hino, S. Henrys, S. Y. Schwartz, and A. F. Sheehan (2016). Slow slip near the trench at the Hikurangi subduction zone, New Zealand, *Science* **352,** no. 6286, doi: 10.1126/science.aaf2349.
Wessel, P., and W. H. F. Smith (1998). New, improved version of the generic mapping tools released, *EOS Trans. AGU* **79,** 579, doi: 10.1029/98EO00426.
Yamashita, Y., H. Yakiwara, Y. Asano, H. Shimizu, K. Uchida, S. Hirano, K. Umakoshi, H. Miyamachi, M. Nakamoto, M. Fukui, *et al.* (2015). Migrating tremor off southern Kyushu as evidence for slow slip of a shallow subduction interface, *Science* **348,** no. 6235, 676–679, doi: 10.1126/science.aaa4242.
Zhang, H., and C. H. Thurber (2003). Double-difference tomography: The method and its application to the Hayward fault, California, *Bull. Seismol. Soc. Am.* **93,** 1175–1189.

Víctor M. Cruz-Atienza
Vladimir Kostoglodov
Vala Hjörleifsdóttir
Arturo Iglesias
Marco Calò
Jorge Real
Allen Husker
Carlos Mortera-Gutierrez

Instituto de Geofísica
Universidad Nacional Autónoma de México
Mexico City, Mexico
cruz@geofisica.unam.mx

Yoshihiro Ito
Takuya Nishimura
Soliman García
Disaster Prevention Research Institute
Kyoto University
Kyoto, Japan
ito.yoshihiro.4w@kyoto-u.ac.jp

Josué Tago
Facultad de Ingeniería
Universidad Nacional Autónoma de México
Mexico City, Mexico

Satoshi Ide
Department of Earth and Planetary Physics
The University of Tokyo
Tokyo, Japan

Masanao Shinohara
Earthquake Research Institute
The University of Tokyo
Tokyo, Japan

Motoyuki Kido
Research Center for Prediction of Earthquakes and Volcanic Eruptions
Tohoku University
Sendai, Japan

Published Online 23 May 2018